npj | climate and atmospheric science

Article

Published in partnership with CECCR at King Abdulaziz University

https://doi.org/10.1038/s41612-026-01383-y

Large present-day and future climate forcing due to non-CO_2 emissions from global transport

Johannes Hendricks[1] ✉, Mattia Righi[1], Sabine Brinkop[1], Katrin Dahlmann[1], Mariano Mertens[1,2], Christof G. Beer[1], Volker Grewe[1,2], J. Christopher Kaiser[1] & Michael Ponater[1]

Emissions from land-based transport, aviation, and shipping contribute significantly to climate change. Besides CO_2, these emissions include short-lived compounds that affect air quality but are also climatically relevant. We use a global chemistry-climate model to show that the climate effects of these non-CO_2 emissions are substantial across all transport sectors both now and in the future. In sum, the non-CO_2 impacts result in a cooling, which offsets the positive climate forcing from transport-induced CO_2 by around 80% at present and between 25 and 60% in different scenarios for 2050. The trade-off that air pollutants mitigate global warming is strongly reduced in a future scenario with low anthropogenic emissions, where even small remaining amounts of non-CO_2 compounds cause significant cooling as they are released in a very clean atmosphere. Our findings emphasize the need to take non-CO_2 effects into account when assessing climate protection strategies for the transport sectors.

Transport of passengers and goods is a fundamental need of our society. Emissions from the transport sectors are, however, one of the major drivers of climate change, both via CO_2 and other climate forcers[1–3]. According to Gidden et al.[2], the annual CO_2 emissions of the global transport system in 2015, the reference year of many current assessments, amounted to 7.9 Gt, contributing about one-fifth to total anthropogenic CO_2 emissions. Land-based transport, aviation, and international shipping accounted for 77.5%, 9.7%, and 12.8% of these emissions, respectively. Transport volumes are expected to grow substantially in the future, which implies particular challenges for climate protection strategies. In the current ambition scenario described by the International Transport Forum (ITF)[4], global demand for passenger and freight transport roughly doubles from 2015 to 2050. The ITF also demonstrates that rigorous mitigation measures are required to reach the emission targets for the transport sectors as determined by the Intergovernmental Panel on Climate Change (IPCC)[5] to limit global warming to 1.5 °C. In the recent scenarios considered by the IPCC[2,3], transport CO_2 emissions continue to grow until 2050, with the exception of those scenarios characterized by stringent mitigation.

In case of road transport and shipping, climate protection strategies predominantly target long-lived greenhouse gases, with a particular focus on CO_2[6–8]. Transport emissions, however, also include short-lived species, such as nitrogen oxides or particulate matter, which we refer to here as non-CO_2 emissions. While CO_2 can reside in the atmosphere for centuries to millennia, the short-lived species show typical residence times of only a few days to months. Due to their adverse effects on human health[8–10], short-lived emission components are mainly subject to mitigation measures for improving air quality[6–8]. In the aviation sector, such components are also targeted by climate protection efforts[11] as their climate forcing, i.e., the extent to which they change the Earth's radiation balance and thus induce climate change, is considered to be of the same order of magnitude as the effect of the CO_2 emissions[12–14]. Compared to other anthropogenic emission sources, the transport sectors show some special characteristics. Shipping and aviation, in particular, often emit into comparatively unpolluted environments, which could imply a high sensitivity of climate to non-CO_2 emissions, as a large relative impact on local concentrations is to be expected. Land transport is a particularly strong contributor to non-CO_2 species, especially nitrogen oxides[1,2,15] and in certain regions, e.g., North America and Europe, also particulate matter[16]. This raises the question of the climate impact of these species, specifically in the context of mitigation strategies. Many studies have therefore focused specifically on the non-CO_2 climate effects of transport, also motivated by the need for information supporting discussions on the choice of the appropriate transport modes for freight and passengers. The existing studies reveal significant climate effects caused by non-CO_2 species not only in the case of aviation[12–14], but also for land-based transport[17–21] and international shipping[18–26]. The emission of short-lived trace gases, in particular NO_x (NO and NO_2), carbon monoxide (CO), and

[1]Deutsches Zentrum für Luft- und Raumfahrt (DLR), Institut für Physik der Atmosphäre, Oberpfaffenhofen, Germany. [2]Faculty of Aerospace Engineering, Section Operations & Environment, Delft University of Technology, Delft, The Netherlands. ✉e-mail: Johannes.Hendricks@DLR.de

non-methane volatile organic compounds (NMVOC), induce climate relevant perturbations of ozone (O_3) and methane (CH_4), both important greenhouse gases. In addition, emitted aerosol particles (e.g., composed of sulfuric acid or black and organic carbon) and aerosol precursor gases (e.g., SO_2, NO_x, and NMVOC) contribute to climate change via modifications of clouds and radiation fluxes. Some short-lived components, such as sulfur compounds, induce a negative global climate forcing, i.e., a cooling effect, which, to some degree, counteracts global warming. While reductions in such species are beneficial for improving air quality, they are potentially counterproductive for mitigating climate change. Such trade-offs are of particular importance, for instance, for designing mitigation strategies for international shipping where sulfur emissions are responsible for severe air pollution in coastal areas and, at the same time, cause a comparatively strong negative climate forcing[20,24–27].

Due to their long residence times, long-lived greenhouse gases are typically well-mixed and, therefore, distributed rather homogeneously in the global atmosphere. In contrast, the short-lived species show strong spatial and temporal variations controlled by their source distributions, atmospheric transport patterns, chemical and microphysical transformations, as well as removal processes. Hence, for assessing the role of short-lived species in the climate system, three-dimensional global chemistry-climate models are required, including representations of all these details[28]. Such models are typically applied to quantify the total anthropogenic climate impact by simulating the changing atmosphere from pre-industrial times to present-day and along possible future scenario pathways. The models can also help to trace the causes of climate change back to the effects of individual emission sectors and processes. However, due to huge computational expenses, not all details can be analyzed, not even on supercomputing facilities. Despite this limitation, several model-based studies have addressed the climate forcing of short-lived compounds from transport[14,17–26], focusing on specific transport sectors, i.e., land-based transport, shipping or aviation, or specific short-lived climate forcers, such as ozone or aerosol particles. However, a complete, self-consistent picture of the transport climate effects cannot be derived from these studies, as very different models were applied and different emission inventories and time horizons were considered. The limited comparability of these results makes it difficult to draw general conclusions about the significance of the various effects. In principle, self-consistent attributions of anthropogenic climate change to specific sectors and emission components could be achieved on the basis of computationally efficient simplified climate models[29,30]. However, such models cannot capture the full complexity and the numerous interactions of all processes driving the climate impact of short-lived emission compounds. To fully account for this, the application of detailed three-dimensional models is necessary. In a previous transport assessment[31], such simulations were performed in a self-consistent manner to assess several effects of the global transport emissions in the year 2000, but complemented by results from other studies, particularly for the aviation sector and the effects of aerosols on clouds. Hence, a consistent quantification of all relevant effects of the transport sectors with a detailed modelling approach is still lacking. For assessments of potential mitigation strategies, also quantifications of the corresponding effects along possible future emission pathways are urgently required.

In the present study, we apply a comprehensive three-dimensional chemistry-climate model to quantify the individual climate effects of the short-lived compounds consistently for all three transport sectors. The calculations are complemented by quantifications of the climate impact of the corresponding CO_2 emissions and changes in methane caused by the chemical perturbations. All effects are investigated using fully consistent emission data sets from pre-industrial times to the year 2015 and up to 2050 in three future scenarios following the Shared Socioeconomic Pathways (SSPs) developed for the IPCC sixth assessment report[2,32,33]. We combine the obtained results to provide, for the first time, a complete and consistent assessment of all relevant transport effects, including those of transport-induced changes in aerosol particles, ozone, methane, and CO_2, based on detailed chemistry-climate model simulations for current conditions and various future scenarios. The present study is accompanied by two publications[15,16] that provide additional details on our simulations of the non-CO_2 effects and the methodical innovations of the underlying chemistry-climate model.

We show that non-CO_2 climate effects are of fundamental importance for all three transport sectors under present-day conditions and for all future pathways considered. For land-based transport and shipping, the non-CO_2 effects entail a significant overall cooling that counteracts the CO_2-induced warming. Compared to the effect of CO_2 alone, this leads to a reduction in the climate forcing of transport as a whole, i.e., when considering the sum of all three transport sectors. For the year 2015, this compensation effect is particularly large (around 80%), and even in the future scenarios, it ranges between about 25% and 60%. As the non-CO_2 species mostly act as air pollutants, which should be urgently avoided, a dilemma arises: mitigating these compounds results in enhanced climate warming. This, in turn, must be compensated for by further intensifying measures for avoiding CO_2. We demonstrate that such trade-offs can be reduced, and climate protection and air pollution control can be reconciled in a future scenario with very low anthropogenic pollutant emissions. In this scenario, only very small amounts of transport-related non-CO_2 emissions occur. However, they still cause considerable cooling, as they are released in a very clean atmosphere. Our results clearly show that climate protection strategies for the transport sectors must take into account both CO_2 and non-CO_2 emission components.

Results

Scenarios and emissions

We consider SSP emission data[2,34] for the year 2015 as the reference state and for different possible future pathways. High computing resources are required to describe the individual effects of all different emission components and transport sectors along these pathways. To keep the computational effort manageable, we focus on the year 2050 rather than on transient calculations until 2100, the final year of the SSPs. This allows for a mid-term view into the future without the limitations resulting from comparatively large uncertainties inherent in longer-term projections.

To span a range of possible effects, we consider three different future scenarios as described in Table 1: the 'middle-of-the-road' scenario SSP2[35] and two contrasting scenarios, SSP1[36–38] and SSP3[39]. For each SSP, different variants are available[2,32,33]. Here, we choose the specific scenario variants applied in the context of the Coupled Model Intercomparison Project Phase 6 (CMIP6)[2,40], for which global gridded emission data are available[34], a prerequisite for simulating the effects of short-lived compounds. As shown in Table 1, we consider the scenarios SSP1-1.9, SSP2-4.5, and SSP3-7.0, which are characterized by an increase in global mean surface temperature of about 1.4 °C, 2.7 °C, and 3.6 °C, respectively, by the end of this century compared to the 1850–1900 average[3]. The scenarios cover a particularly wide range of non-CO_2 emissions in 2050.

The changes in the annual emissions of the different climate-active compounds from global land-based transport, aviation, and international shipping between 2015 and 2050 in the different scenarios are shown in Fig. 1. SSP1-1.9 (green) shows strong reductions in the emissions of all compounds, especially in land-based transport by assuming i) strong technological progress leading to improvements in efficiency and exhaust gas-treatment, ii) a growing market share of sustainable alternative fuels, iii) a significant growth of electrified mobility based on renewable energy, and iv) comparatively high shares of public transport. In most cases, aviation and shipping also show a significant emission decrease due to the use of sustainable alternative fuels and new technologies. These reductions, however, are smaller compared to land-based transport. As a consequence of air pollution control measures, the emissions of short-lived compounds from land-based transport in SSP2-4.5 (blue) are also declining until 2050, but the reductions are significantly smaller than in SSP1-1.9. In contrast to SSP1-1.9, CO_2 from land-based transport increases in SSP2-4.5. Such differences are due to the continued use of fossil fuels and less technological progress in the SSP2 scenario. CO_2 from the shipping sector shows a similar behavior.

Table 1 | Summary of the scenarios used in this analysis

Scenario	Description
SSP1-1.9[2,36–38]	Sustainability scenario: strong economic growth, but very sustainable fuel pathways resulting in substantial emission reductions in order to limit global warming to less than 1.5 °C in 2100; change in global mean surface temperature by the end of the century: ΔT = 1.4 (1.0 to 1.8) °C
SSP2-4.5[2,35]	Middle-of-the-road scenario: moderate population growth; continued use of fossil fuels at similar levels as today, leading to continued increase of greenhouse gas emissions; continuation of air pollution reduction according to current developments, leading to decreases in emissions of short-lived compounds in developed and developing countries; change in global mean surface temperature by end of the century: ΔT = 2.7 (2.1 to 3.5) °C
SSP3-7.0[2,39]	Regional rivalry scenario: future with high inequality between regions; countries increasingly focus on domestic or regional issues; decrease in global trade and international cooperation; increase in global gross domestic product (GDP) small and concentrated in currently high-income nations; population increase mainly in low- and middle-income countries; resurgence of coal use in energy systems; control of air pollutant and greenhouse gas emissions less effective leading to increased emissions of both short-lived compounds and long-lived greenhouse gases; change in global mean surface temperature by end of century: ΔT = 3.6 (2.8 to 4.6) °C

In the naming of the scenarios (SSPx-y), x indicates the basic scenario narrative and y refers to the approximate radiative forcing (W/m^2) in the year 2100 induced by anthropogenic emissions when compared to pre-industrial times. The radiative forcing denotes the global mean change in energy flux in the atmosphere caused by the emissions (the values here correspond to the changes in energy flux in 2100 compared to 1750). Different variants y were developed for each scenario group x. ΔT denotes the long-term change in global mean surface temperature (2081-2100 average compared to 1850-1900 average)[2]. Quoted ΔT values are the best estimate values and the very likely ranges in parentheses.

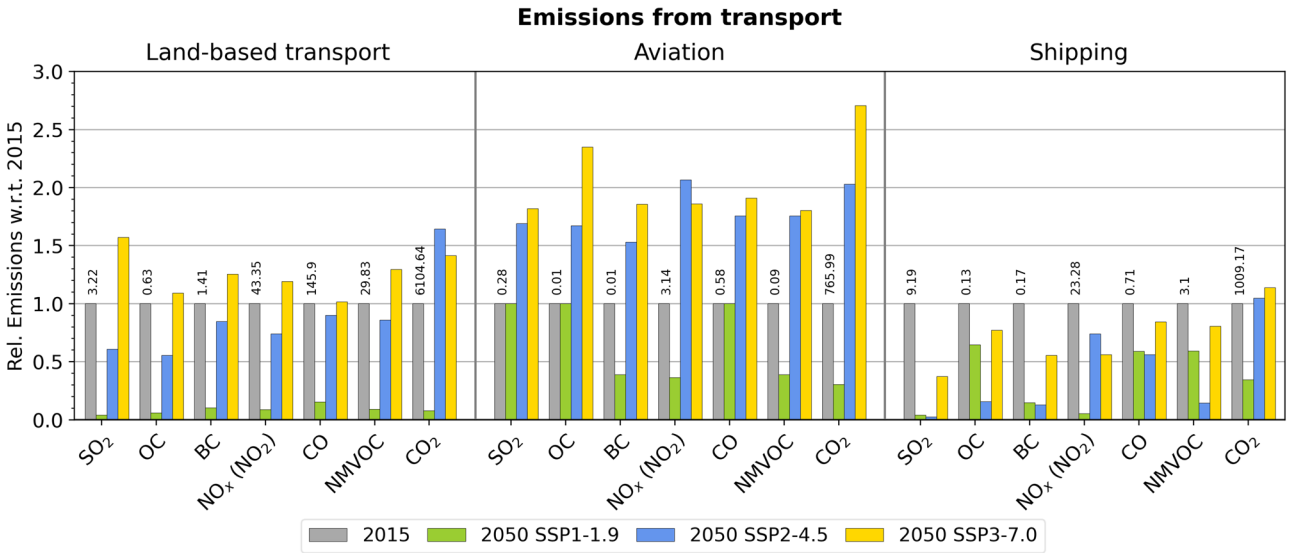

Fig. 1 | Global emissions of climate-active compounds in 2015 and 2050 in the SSP scenarios. Annual global emissions of land-based transport, aviation, and international shipping in 2050 in SSP1-1.9 (green), SSP2-4.5 (blue), and SSP3-7.0 (yellow) relative to the 2015 emissions. The total amount of emissions (given in Tg, with NO_x expressed as NO_2) in 2015, taken from the SSP2-4.5 database is indicated for each species on top of the grey bars. Note that the different compounds show very different climate forcings per unit of emitted mass. Therefore, comparing the emission levels of different compounds is unsuitable for assessing their effects on the climate. OC and BC denote particulate organic and black carbon, respectively. NMVOC stands for non-methane volatile organic compounds. The CO_2 emissions do not include the contribution from the use of biomass-based fuels, due to the assumed net-zero effect on atmospheric CO_2. Emissions of CH_4 are not considered, since they are low in the investigated cases. Normalizing to 2015 ensures the comparability of the emission components with regard to their future development. Further information on the emission data applied is provided in the 'Methods' section. Note that for the calculation of the transport-induced climate effects of CO_2 and CH_4, the full time series of the relevant emissions is applied, including historic emissions before 2015 (see also 'Methods' section). For the absolute numbers and details on the spatial distribution of the emissions in 2015 and the future scenarios, we refer to the Supplementary information (Supplementary Table 1 and Supplementary Figs. 1–3).

Importantly, SO_2 emissions from shipping exhibit a similarly strong reduction in SSP2-4.5 as in SSP1-1.9 due to efficient regulations of the maximum fuel sulfur content[41]. In contrast, aviation emissions in SSP2-4.5 strongly increase for all components by 2050 due to high growth rates of transport volumes and less stringent emission control. In SSP3-7.0 (yellow), emission control is less restrictive than in the other SSPs, leading to the largest increases in the emissions of nearly all short-lived components in the case of land-based transport and aviation by 2050. CO_2 from land-based transport, however, shows a smaller increase than in SSP2-4.5 due to the smaller growth rates assumed in SSP3 (Table 1). For the shipping sector, SSP3-7.0 shows the highest emissions in 2050 among all three scenarios, but the emissions of short-lived compounds are lower compared to 2015. Especially for SO_2, this results from the above-mentioned emission control regulations, which already entered into force shortly after 2015[41] and, therefore, are only weakly affected by the specific long-term development of the scenario.

The present study focuses on the direct transport emissions only, i.e., emissions directly released by road vehicles, aircraft, and ships. The electrification of mobility could potentially cause a shift of emissions into the energy sector, if power generation is not fully covered by renewable energy, or even into other sectors, such as industry, due to changes in vehicle production and energy provisioning technology. Since electrification of the transport system was negligible in 2015 and the contribution of electricity to global transport final energy is still comparatively low (around 5%) in 2050 in SSP2-4.5 and SSP3-7.0[36], this effect is of secondary importance in these cases, and trade-offs due to sectoral shifts of emissions are probably small. In order to minimize greenhouse gas emissions and their climate effects, SSP1-1.9 assumes a rapid increase in renewable energy, stringent emission

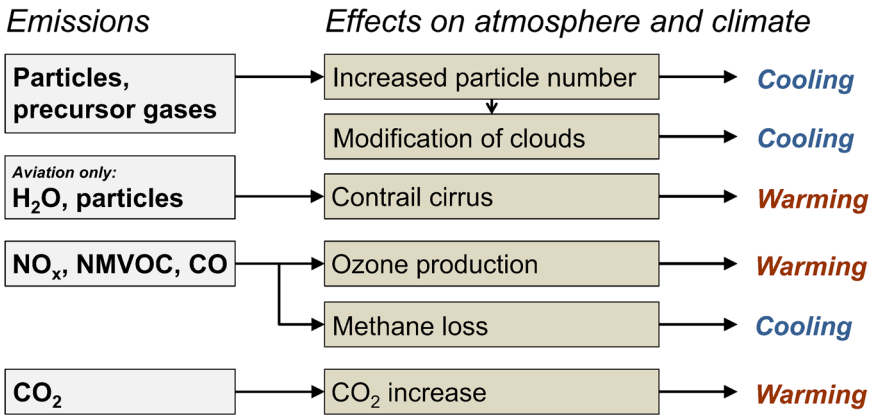

Fig. 2 | Schematic overview of the effects of the individual transport emission components on the atmosphere and climate. Major effects of transport-induced emissions of aerosol particles (e.g., sulfate particles or soot consisting of mixtures of BC and OC), particle precursor gases (e.g., SO_2, NO_x, NMVOC), ozone precursor gases (NO_x, NMVOC, CO), and CO_2 are shown. In addition, the contrail formation effect is indicated for the aviation sector. Beyond the warming by CO_2, the non-CO_2 effects have important implications for the climate. Emitted aerosol particles interact with radiation and clouds, which, in most cases, leads to increased back-scattering of solar radiation into space. This results in a cooling, which on average overcompensates the warming effect caused by the absorption of radiation by emitted soot. These effects are further amplified by the production of particulate matter from emitted precursor gases. An additional effect occurs in the case of aviation, where emissions of water vapor and aerosol particles induce contrail cirrus clouds, which results in a warming. Emissions of specific trace gases, particularly NO_x, NMVOC, and CO, lead to the production of atmospheric ozone. Since ozone is a greenhouse gas, in addition to its well-known ability to absorb harmful UV radiation, this amplifies global warming. Another effect of the trace gas emissions is the chemical loss of the greenhouse gas methane (CH_4), leading to cooling that counteracts the ozone-induced warming. The methane loss further results in chemical feedbacks, such as the reduction of ozone production, which further amplifies the cooling effect. Direct CH_4 emissions, which can result, for instance, from the use of liquefied natural gas in shipping[76], are not considered since they are low in all scenarios investigated in this study. The described effects of non-CO_2 compounds represent long-term global mean changes that are to be expected in most of the cases considered. Note that the non-CO_2 effects can vary strongly depending on location, time of day, and the background conditions.

control, and decarbonization, including carbon capture and storage (CCS). Hence, a shift of emissions to other sectors can be expected to be small in the case of CO_2. In addition, SSP1-1.9 assumes rapid future emission reductions not only for CO_2 but also for non-CO_2 emissions for most species and sectors[2]. This indicates that possible trade-offs are probably small also in this scenario.

Effects on atmosphere and climate

A schematic overview of the typical effects of the various emission components on the atmosphere and the climate is provided in Fig. 2, based on existing literature (see Introduction). In addition to the warming caused by CO_2 emissions, a number of climate-relevant processes are induced by short-lived emission components. Some of them increase global warming, while others have a cooling effect, in particular aerosol particles and the chemical loss of atmospheric methane.

The climate forcing due to anthropogenic emissions has traditionally been described by the radiative forcing (RF) metric, which describes the global mean change in the Earth's radiation budget induced by atmospheric perturbations, such as concentration changes of greenhouse gases, as a result of the emissions[42,43]. A positive RF implies an increase in the global mean atmospheric near-surface temperature (warming), a negative RF a decrease (cooling). A related, more advanced metric is the effective radiative forcing[42–44] (ERF), which also accounts for the effects of rapid adjustments as a result of the initial perturbation, such as changes in clouds or water vapor, which are not covered by the classical RF formulation. Since these rapid adjustments can have an important influence on the climate response to the emissions, we use the ERF as a metric for the expected climate change. In the case of transport-induced changes in the concentrations of short-lived species, such as aerosols or ozone, the corresponding ERF needs to be calculated on the basis of their spatial distributions, as these exhibit a large variability (see results from our model simulations presented in Supplementary Figs. 4–23). The spatial distributions of the aerosol perturbations simulated in this study roughly match those of the emissions, but show a distinct dispersion following the dominating wind patterns. The distributions of transport-induced ozone are characterized by a stronger spatial dispersion due to a longer atmospheric residence time of ozone compared to particles. For a more detailed analysis of the spatial variability of the transport effects, we refer to the two accompanying papers[15,16]. In contrast to the short-lived compounds, long-lived greenhouse gases show nearly homogeneous spatial distributions, which allows for radiative forcing calculations based on global mean concentration changes.

Effects of land-based transport

Figure 3 shows our ERF results for the different atmospheric perturbations in 2015 and 2050 caused by global transport emissions from pre-industrial times to the respective year. In the case of land-based transport, the CO_2 ERF has the largest contribution. The calculated values increase from 315 mW/m^2 in 2015 to up to 606 mW/m^2 in 2050 in SSP2-4.5. A comparison of these numbers to the corresponding total anthropogenic radiative forcing[2] of about 2.4 W/m^2 and 3.7 W/m^2, respectively, including all anthropogenic effects, demonstrates that land-based transport is an important contributor to global warming. In contrast to the emissions (Fig. 1), the ERF of CO_2 in 2050 shows no decrease in SSP1-1.9. This is due to the very long atmospheric residence time of CO_2, resulting in a long-term accumulation. Therefore, the decrease in emissions from 2015 to 2050 only results in a reduced increase in the atmospheric burden of transport-induced CO_2 and the corresponding ERF, but not in a decrease. Aerosols from land-based transport emissions induce a negative ERF, which is mainly caused by an increase in aerosol particle mass and number concentration that induce cloud perturbations[16]. The simulated aerosol ERF amounts to -164 mW/m^2 in 2015. The future development closely follows the development of the emissions of the major aerosol precursors SO_2 and NO_x as well as the primary aerosol components OC and BC. The aerosol-induced 2050 ERF ranges between a negligible value in SSP1-1.9 and a slight exceedance (absolute values) of the 2015 ERF in SSP3-7.0. The contribution of land-based transport emissions to ozone causes a positive ERF of 118 mW/m^2 in 2015, i.e. a lower value than that of the corresponding absolute aerosol ERF, but with a similar future development that closely follows the emissions of the ozone precursor gases NO_x, CO, and NMVOC. The corresponding loss of methane results in a negative ERF, which tends to slightly overcompensate for the warming effect of the ozone formation, induced by the same emitted species. This is an important new finding that results from the

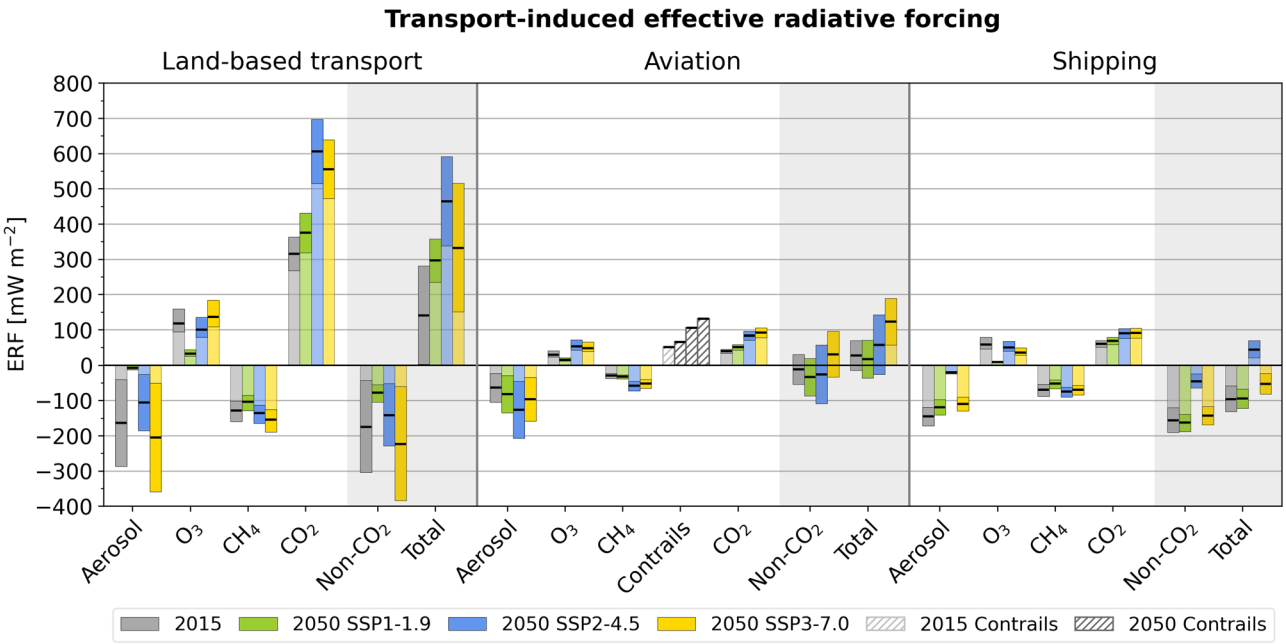

Fig. 3 | Effective radiative forcings (ERF) induced by the emissions of the different transport sectors from pre-industrial times to 2015 and 2050 for three SSP scenarios. Effective radiative forcing (in milliwatts per square meter) due to changes in atmospheric aerosol particles, ozone (O_3), methane (CH_4), and CO_2, induced by the emissions of global land-based transport, aviation, and international shipping in 2015 (grey) as well as in 2050 in SSP1-1.9 (green), SSP2-4.5 (blue), and SSP3-7.0 (yellow). In addition, the total non-CO_2 effect and the total ERF (sums of all contributing ERFs), both including contrails in the case of aviation, are shown for each transport sector (grey shaded areas). The computed multi-year average values are indicated by the thick horizontal lines within the bars. Corresponding uncertainties (see 'Methods') are displayed by dark shadings at the end of each bar. The ERF of CH_4 includes the effect of long-term ozone modifications caused by transport-induced CH_4 changes. Note that the comparatively small aerosol ERFs simulated for land-based transport in 2050 in SSP1-1.9 and for shipping in 2050 in SSP2-4.5 are statistically not significant[16] and contribute only marginally to the total transport effects. The aviation contrail cirrus effect could not be simulated in this study, due to a lack of required input data in the CMIP6 emission data set, specifically data on the flown distances and on the emission of water vapor. Instead, values derived from the literature are displayed ("Contrails"). In addition to the contrail cirrus ERF reference value for 2015, values for 2050 were determined with different assumptions regarding the degree of sustainability in correspondence to the respective SSP scenario (see 'Methods'). A list of all ERF values is provided in Supplementary Table 2.

application of a new method (see below). Earlier studies showed a significantly smaller methane effect[31]. A striking outcome is the methane ERF in SSP1-1.9, which is still large despite the strong reductions in the responsible emissions, for instance, of NO_x. This results from the non-linearity in the dependence of the atmospheric oxidation capacity on NO_x, with the highest increase due to emissions of NO_x under clean background conditions[45]. It implies that, in very clean environments, even low transport-induced emissions can result in significant climate perturbations. A similar effect could potentially also occur in the case of other anthropogenic land-based NO_x emissions under clean background conditions, as they are often co-located with transport emission sources and result in similar chemical perturbations. The present-day ERF values due to the changes in aerosols, ozone, and methane induced by land-based transport, as quantified here, are significantly higher (typically around a factor of 2) than estimated in earlier studies[17,18,20,31]. This mainly results from revised assumptions on aerosol particle number emissions[46] and the application of a tagging approach for quantifying transport-induced contributions to ozone and methane (see 'Methods'). In the case of ozone and methane, updates of the emission data also play an important role.

A striking feature is that the total non-CO_2 effect of land-based transport is a cooling (Fig. 3, light-grey shaded area), which compensates for a significant fraction of the CO_2-induced warming. In 2015, this resulted in a total ERF from land-based transport, which is 56% lower than the ERF of CO_2 alone. The importance of non-CO_2 compounds relative to CO_2 is strongly influenced by the development of the CO_2 emissions from pre-industrial times to the year in focus. Due to the long residence time of CO_2 in the atmosphere, a prolonged emission period results in a more pronounced CO_2 effect. This can reduce the relative effects of the non-CO_2 species in the future scenarios. However, in 2050, the reduction in the total ERF due to the non-CO_2 cooling effect, compared to the ERF of CO_2 alone, still amounts to 21%, 23%, and 40% in SSPs 1-1.9, 2-4.5, and 3-7.0, respectively. This indicates the particular importance of non-CO_2 compounds for the climate effects of emissions from transport, also in future projections.

Effects of aviation and shipping

The characteristics of the climate effects of aviation and shipping shown in Fig. 3 are partly different from those of land-based transport. While the signs of the various effects are the same as in the case of land-based transport, with cooling aerosol and methane effects and ozone-induced warming, the total ERFs of aviation and shipping are significantly lower. Furthermore, the ERF from CO_2 is not the dominant forcing. In many cases, the non-CO_2 effects are of similar magnitude or even larger. This results from the responsible processes being particularly efficient in comparatively clean air, as found at the typical flight altitudes and over the open ocean. In addition, differences in the sizes of emitted particles, which vary among the sectors, are important[20]. The ERF per unit of emitted mass of the respective substances, the so-called ERF efficiency (Table 2), can therefore be significantly higher than for land-based transport. Due to the very clean conditions at aircraft cruise levels in many parts of the world, this effect is particularly large in the case of the aviation-induced aerosol effect, where the ERF efficiency is about 10 to 20 times higher than for emissions from land-based transport. As a result, aviation shows an aerosol ERF of similar magnitude to that of the other sectors, while the emissions of aerosol particles and particle precursor gases from aviation are only low (Fig. 1, Supplementary Table 1). In the case of shipping, a particularly high aerosol ERF efficiency occurs in 2050 in SSP1-1.9, which is a consequence of the comparatively low total aerosol concentrations over remote marine areas and the resulting distinctively larger shipping-induced relative increases in cloud-forming aerosol particles[16].

Table 2 | Effective radiative forcing efficiencies of transport-induced effects of short-lived species emissions in 2015 and 2050 in the SSP scenarios

ERF_{eff} (mW/m²/Tg[species]/yr)		2015	2050		
Sector	Parameter		SSP1-1.9	SSP2-4.5	SSP3-7.0
Land-based transport	Aerosol	−49.68	*−31.89*	−45.83	−46.28
	O_3	4.06	13.06	4.65	3.92
	CH_4	−0.49	−3.09	−0.67	−0.50
Aviation	Aerosol	−508.74	−695.09	−603.06	−418.07
	O_3	14.73	20.96	12.70	12.78
	CH_4	−1.67	−4.31	−1.60	−1.59
Shipping	Aerosol	−37.47	−476.79	*−154.33*	−71.95
	O_3	3.79	11.51	4.40	4.17
	CH_4	−0.46	−2.40	−0.75	−0.84

The ERF efficiencies (ERF_{eff}) are defined as the ratio between the respective ERF and the emitted amount of the substance inducing the ERF. In the case of O_3, the ERF efficiency is calculated by dividing ERF(O_3) by the total annual emission of NO_x (expressed as NO)[15] of the respective sector. Due to the long lifetime of atmospheric methane (about 9 years[58,62]), ERF(CH_4) can also be influenced by chemical loss processes in the years before 2015 and 2050, respectively. Therefore, we calculate the ERF efficiency of methane as the quotient of ERF(CH_4) and the NO_x emissions of the 9 years up to the analysis year (2007–2015 and 2042–2050, respectively). In the case of aerosol, the ERF values were divided by the sum of the annual emissions of particulate matter (BC and OC) and a fraction of the aerosol precursor gas SO_2. Here we consider a mean fraction of SO_2 converted to aerosol sulfate by gas-phase (17%) and liquid-phase (33%) chemistry[74], whereby one third of the latter is not taken into account as this fraction is typically removed directly by precipitation[75]. Overall, this results in a converted share of 39%. Aerosol nitrate formed from NO_x emissions is not considered due to its semivolatile character. Numbers shown in italic represent statistically not significant values[16]. The values shown can slightly deviate from the ratios of the ERF and the corresponding globally aggregated emissions listed in Supplementary Tables 1 and 2; here we use aggregated emissions calculated from the gridded emissions preprocessed for application in the applied chemistry-climate model (see 'Methods'), which slightly differ from the corresponding original CMIP6 values, due to the applied regridding and tagging procedures (maximum deviations around 3%). ERF efficiencies for CO_2 were not considered due to its very long atmospheric residence time, implying a comparatively homogeneous spatial distribution, which results in only small variability of the ERF efficiency between the transport sectors.

Aviation emissions lead to an aerosol-induced cooling with absolute values exceeding those of the ozone and methane effects (Fig. 3). The aerosol effects are mostly due to aerosol-induced modifications of lower-level clouds following the downward transport of aviation-induced particles[16,20]. We do not consider the possible impact of aviation-induced soot particles on natural cirrus clouds, since a recent study indicated that the effect is small compared to that on lower-level clouds[47]. The ERFs by ozone and methane almost compensate each other, except for SSP1-1.9, where the methane-related ERF is particularly large as a result of a comparatively clean atmosphere. The considered ERF of contrail cirrus (Fig. 3) shows similar absolute values as the aerosol effect, but with a positive sign indicating a warming. Note that the spatial distribution of the radiative effect of contrail cirrus closely follows the respective flight patterns in the regions relevant for this process[48]. On an annual average, contrail cirrus leads to a positive local radiative forcing. Since contrail cirrus ERF could not be simulated here due to a lack of required input parameters in the CMIP6 data, we rely on literature-based ERF values (see 'Methods'). In this context, we emphasize that these ERF values are likely to be quantitatively consistent with the modelling carried out here for the other processes, as indicated by the results of a recent model study (see 'Methods').

Due to compensation effects, the sum of the non-CO_2 effects remains small for aviation, leading to a net warming impact from the aviation sector. The corresponding ERF increases from 27 mW/m² in 2015 to values of 57 mW/m² and 122 mW/m² in 2050 in SSP2-4.5 and SSP3-7.0, respectively. In SSP1-1.9, however, the net warming decreases to 17 mW/m², which is remarkable, given the high growth rates in aviation. The 2015 value is significantly lower than the value of 101 mW/m² reported for 2018 in a recent aviation climate assessment[14]. This is mainly due to the negative aerosol ERF, which was not included in the best estimate of that assessment. The value obtained here for 2015, when excluding the aerosol ERF, amounts to 91 mW/m², which is close to that of the assessment. The remaining discrepancy can be explained by the growth in emissions from 2015 to 2018 and with slight deviations in the non-CO_2 ERFs resulting from methodical differences, e.g., due to the application of a tagging method for the O_3 and CH_4 effects in the present study (see 'Methods'). In addition, the use of a single model system, allowing for a consistent treatment of emissions and sectors, might lead to deviations from the results derived from a large model ensemble in the assessment.

Shipping emissions led to a strong cooling effect by aerosols in 2015 (Fig. 3), consistent with other model studies[20,22,24,25] performed for the conditions before 2020, when strong sulfur emission reductions in international shipping[41] were enforced. For 2015, we obtain an aerosol-induced ERF of −146 mW/m². This value is only moderately reduced by 2050 in SSP3-7.0, where less strict emission regulations are assumed than in the other scenarios. Strong sulfur emission reductions apply, however, in SSP2-4.5 and SSP1-1.9. While SSP2-4.5 shows a corresponding strong reduction in the ERF, a striking feature occurs in SSP1-1.9, where the ERF is still large. This is the result of the high ERF efficiency in SSP1-1.9 discussed above (Table 2), i.e. a strong effective radiative forcing despite low emissions. This is also the case for the shipping-induced reduction of CH_4, where in SSP1-1.9 in 2050 the ERF is still large (−53 mW/m²) compared to 2015 (−70 mW/m²) despite strong reductions in NO_x emissions from shipping. The shipping-induced ERF of the CH_4 loss overcompensates that of the corresponding increase in O_3 in all cases. In combination with the aerosol-induced cooling and the comparatively small ERF of CO_2, this results in a negative value of the total ERF from shipping emissions except for SSP2-4.5 in 2050, which shows a small positive total ERF. Hence, in contrast to land-based transport and aviation, shipping tends to induce a cooling in most cases. The net warming in SSP2-4.5 is caused by the strongly reduced aerosol cooling, which can be expected as a consequence of sulfur emission reduction in shipping and a pollution level similar to present-day conditions[24,25]. Recently, it has been demonstrated that the radiative forcing of cloud modifications in the form of invisible ship tracks could further amplify the ship-induced cooling and that this could potentially lead to an even stronger effect than the large-scale cloud modifications investigated here[49]. This further underlines the importance of particles from shipping in the ongoing discussion of mitigating the climate effects of transport emissions.

Effects of the total transport system

The ERF of the total transport system, calculated as the sum of the ERFs of the individual transport sectors, is shown in Fig. 4. The total transport-induced ERF of CO_2 amounts to 415 mW/m² in 2015. This is about one-fifth of the corresponding ERF of total anthropogenic CO_2[44], which emphasizes the importance of the transport sectors in climate change. The transport-induced CO_2 effect increases by 2050 in proportion to the additional CO_2 emissions released in the respective scenarios in the time period from 2015 to 2050. Despite the large importance of CO_2, the total ERF of all transport sectors and species is significantly smaller than the ERF of CO_2 alone, caused by the net-cooling of the non-CO_2 climate forcers. The cooling by aerosols, with a corresponding ERF of -373 mW/m² in 2015, strongly contributes to this effect. Compared to the ERF of all anthropogenic aerosols of −1.16 W/m² calculated with the same model for 2014[47], the 2015 value also reveals the high relevance of transport emissions. While the negative aerosol ERF of total transport slightly increases by 2050 in SSP3-7.0 (10% larger absolute value), the other two SSPs show a reduced, but still very significant ERF (56% and 68% of the 2015 value in SSP1-1.9 and SSP2-4.5, respectively). The positive ERF of ozone induced by total transport emissions in 2015 is slightly overcompensated by the corresponding negative methane loss ERF resulting from the same emission components. This is also the case in 2050 in SSP2-4.5 and SSP3-7.0, leading to a very small sum of

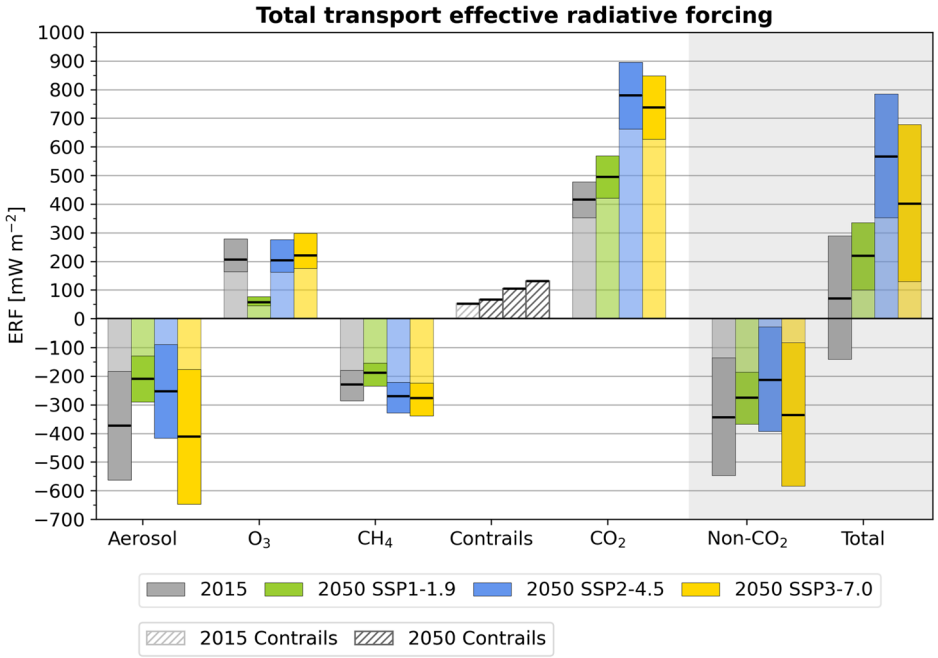

Fig. 4 | Effective radiative forcing of atmospheric effects induced by the total emissions of global transport from pre-industrial times to 2015 and 2050 in the SSP scenarios. As Fig. 3, but for the total effect of transport calculated as the sum of the ERFs from land-based transport, aviation, and shipping.

the ozone and methane effects. Only in SSP1-1.9 a comparatively strong methane effect leads to a significant net cooling of the combined ozone and methane ERFs. The cooling effect of the summed non-CO_2 forcings reduces the total transport ERF compared to the effect of CO_2 alone. This reduction is particularly large in 2015 (83% reduction) and still very significant in 2050 (56%, 27%, and 46% in SSPs1-1.9, 2-4.5 and 3-7.0, respectively). Therefore, the non-CO_2 contributions are highly important both, at present-day and in the future scenarios, including the low-emission scenario SSP1-1.9, where this might not be expected, given the very low emissions of non-CO_2 species in this scenario.

In view of the high relevance of the non-CO_2 emissions, we stress that the quantification of their climate forcing is complex and, therefore, suffers from uncertainties[43] (see also Figs. 3 and 4). Specific uncertainties in quantifying the effects of transport-induced aerosol particles and short-lived gases have been discussed in our previous studies[20,21] and are the subject of the accompanying papers[15,16].

Discussion

The consistent simulation of the variety of transport emission effects performed in this study allows for a direct comparison of the individual climate forcings resulting from the different emission components and transport sectors. The results show that the global emissions of land-based transport and aviation significantly contribute to global warming, with land-based transport showing the largest contribution (140 mW/m^2 effective radiative forcing in 2015 compared to 27 mW/m^2 in the case of aviation). In the SSP2-4.5 and SSP3-7.0 future scenario pathways, the positive climate forcing of the two sectors increases from 2015 to 2050. In the case of land-based transport (increase of total ERF by factors of 3.3 in SSP2-4.5 and 2.4 in SSP3-7.0), this is largely due to the additional CO_2 emissions released until 2050. The non-CO_2 emissions of land-based transport have a significant overall cooling impact in all cases considered. Hence, reductions in these emissions could further amplify the warming effect. This occurs in our simulations, for instance, through the strong reduction of the aerosol effect in SSP1-1.9. Comparatively high growth rates in aviation transport volumes lead to a future increase in both the effect of contrail cirrus and that of CO_2, enhancing the sector's warming effect by 2050 (factor of about 2 in SSP2-4.5 and more than 4 in SSP3-7.0). Only in the SSP1-1.9 scenario, a particularly large aerosol-induced cooling reduces the total aviation effect slightly when compared to 2015. Global shipping has a net cooling impact in all simulated cases, except for the SSP2-4.5 scenario. This is a result of the strong cooling effect induced by the non-CO_2 emissions. Due to stringent sulfur emission regulations, the net cooling turns into a warming in SSP2-4.5. A striking phenomenon occurs in SSP1-1.9, where clean background conditions still result in a large cooling effect despite a strong reduction of non-CO_2 emission components. This results from the effects of aerosols and chemical methane loss being particularly efficient under clean atmospheric conditions, which occur when anthropogenic emissions as a whole are strongly reduced.

These results demonstrate the importance of the non-CO_2 transport emissions when quantifying transport-related climate effects. Since global emissions were considered here, we stress, however, that the results are not necessarily transferable to specific regions. In an earlier study[50], for example, we showed that the effects of land-based transport emissions in Germany are dominated by CO_2, which is a consequence of (i) the long history of emissions and the associated long-term accumulation of CO_2 in the atmosphere and (ii) stringent mitigation measures to reduce short-lived components in European transport emissions. The effects of transport emissions from other regions of the world, especially from emerging or threshold countries, can behave differently.

Due to the specific conditions over the oceans and at the main flight altitudes of air traffic, the results obtained for shipping and aviation should not be transferred to other anthropogenic emission sources. In the case of land transport, however, the results of this study could also provide hints on the potential effects of other anthropogenic land-based emission sources of the non-CO_2 species analyzed here. Such sources are often co-located with transport emissions and, consequently, could lead to similar atmospheric perturbations. However, this should be assessed in more detail in future studies.

The present study focuses on the direct vehicle emissions from the transport sector. Since SSP1-1.9 is characterized by fundamental changes in energy supply, fuels, and vehicle technology, the comparison with other future scenarios may have to take into account transport-related changes in emissions from other sectors as well, such as the energy sector, industry or, due to the increased production of biofuels in SSP1, agriculture. Although SSP1-1.9 is characterized by a strong future reduction in emissions of most species and sectors, and possible trade-offs due to fundamental changes in transport-related emissions in other sectors are likely to be small, such effects require a more detailed analysis. Therefore, full life cycle analyses for

Table 3 | Overview of the models applied

Process	Model	Model type
Aerosol effects	EMAC[52] including the aerosol submodel MADE3[16,46,47,53]	3D global chemistry-climate model
Ozone effect and change in methane lifetime	EMAC[52] in QCTM/TAGGING configuration[15,21,55,56]	3D global chemistry-climate model
CO_2 and methane effects	AirClim[59,60] with extensions to include the tagging approach (see main text for details)	climate response model

both fuels and technologies involved, including an adequate assessment of emissions and climate impacts, should be a central topic of future transport-related research.

The results of this study have several other important implications. When comparing scenarios or measures for mitigating the climate impact of transport emissions, the consideration of non-CO_2 components can be crucial, not only for aviation but also for surface-based transport. For ranking measures with a similar CO_2 reduction potential, the non-CO_2 components can be decisive. In cases of a significant cooling effect of non-CO_2 components, their reduction would have to be compensated for by intensifying climate protection measures elsewhere. In discussions about a possible mitigation of global warming through the cooling effect of non-CO_2 emissions, it should be taken into account that these compounds, unlike CO_2, mostly remain in the atmosphere for only a few days to weeks. Hence, as also emphasized in studies on possible geoengineering measures[51], continuous emissions would be required to counteract parts of the CO_2-induced warming. In any case, it is essential to recall that non-CO_2 emissions can strongly reduce air quality[3,6,8–10], and trade-offs between the protection of climate and air quality must be avoided. In case of a strong reduction in total anthropogenic emissions, as occurring in SSP1-1.9, even small residual non-CO_2 emissions from transport can lead to a comparatively large negative climate forcing. In view of such significant emission reductions, these cooling effects would not necessarily be at the expense of air quality. In such cases, the trade-offs between air pollution control and climate protection may not be as critical as it was recently discussed, for instance, for international shipping[24–27]. Consequently, evaluations of mitigation strategies for air pollution control and climate protection in the transport sectors need to consider the overall atmospheric pollution level, and possible trade-offs or co-benefits should be a central subject of discussion. Large effects of transport-induced non-CO_2 components on climate can be expected also for the future and should therefore be taken into account in the design of mitigation measures.

Methods

EMAC simulations: aerosols, ozone and the methane lifetime

All simulations of the effects of short-lived species, i.e., transport-induced aerosol effects, ozone production, and changes in methane lifetime, were performed with the global chemistry-climate model system EMAC[52] (ECHAM/MESSy Atmospheric Chemistry model). Detailed descriptions of these simulations are provided in the accompanying articles[15,16]. In the following, we therefore only provide a brief overview of the methodological details of the EMAC simulations, focusing in particular on the aspects that are especially relevant for this study. EMAC includes several submodels to describe atmospheric processes, their interaction with oceans and land, and to assess human influences. Table 3 provides an overview of the applied EMAC configurations.

For simulating atmospheric aerosol particles and their effects on clouds and radiation, we use a configuration that includes the aerosol submodel MADE3[46] (3rd version of the Modal Aerosol Dynamics model for Europe adapted for global applications) coupled to the EMAC cloud and radiation submodels[16,47,53] on the basis of the calculated aerosol particle number concentration, size distribution, and chemical composition. In a previous study[46], a comprehensive evaluation of the aerosol mass and number concentrations modelled with EMAC, including MADE3 was performed using data from airborne field campaigns, satellite observations, and station networks. A reasonable agreement with the observations was demonstrated. Deviations, such as the underestimation of fine particle deposition or the fact that near-surface particle number concentrations are often lower than those observed from aircraft, are of a similar order of magnitude as in comparable other global modelling studies. In a subsequent work[53], the ability of the model to reproduce the relevant observed cloud and radiation properties was successfully demonstrated.

The effects of transport-induced aerosols are calculated by a perturbation method, which is based on the analysis of the differences between simulations with and without the emissions of the respective transport sector. To ensure statistically significant detection of even small transport-induced differences, the so-called nudging technique is applied, where meteorological model variables are relaxed towards meteorological reanalysis data, to minimize the differences due to their variation between the model simulations. We carried out simulations for a period of 11 years, from 2005 to 2015. The first year is used as model spin-up and is not included in the analysis. The simulations are designed as so-called time slice experiments considering the emissions of a specific year, here 2015 or 2050, as representative for the respective time horizon. These emissions are applied in combination with multi-year meteorological data in order to cover natural variability. In order to isolate the specific effects of the respective transport sector emissions, changes in meteorology due to the changing climate are not considered, as they would mask the pure effects of the emissions. Therefore, the same meteorological data is used for all simulations. A previous study suggests that, on the time scales considered here, effects of climate change are probably smaller than the pure emission effect in the case of the transport impact on ozone and methane[54]. However, it is unclear whether this also holds for aerosol effects. These issues should therefore be re-assessed in future studies. For more detailed information on the performed simulations, we refer to our accompanying article on transport-induced aerosol effects[16].

To calculate the effects of transport emissions on ozone and on the lifetime of atmospheric methane, EMAC is applied using the so-called QCTM/TAGGING configuration[21], including a very detailed description of the atmospheric gas-phase chemistry. The quasi-chemistry-transport model (QCTM) mode decouples atmospheric chemistry from the model dynamics, which facilitates the quantification of the transport emission effects. The TAGGING submodel[55,56] allows for quantifications of the contributions of specific emission sources, such as the transport sectors, to the concentrations of atmospheric chemical compounds. The representation of ozone and other trace gases in the EMAC model was evaluated against observations in detail in an earlier study[52]. It was concluded that EMAC tends to show a positive bias for tropospheric ozone (about 10-50% of the average concentrations in the upper troposphere depending on season and altitude, compared to aircraft-based observations). As discussed in the accompanying article[15], the deviations of the present simulations from those described in the earlier study are very small. Therefore, we refer to this previous article for more information on the model performance with respect to the representation of ozone. With regard to the representation of the methane chemistry, the evaluation of earlier simulations with EMAC revealed that the simulated methane lifetime is typically at the lower end of the values estimated by other comparable models[57]. However, many of the models show a low bias compared to observations. The chemical lifetime of CH_4 simulated in the present study ranges from 7.4 years in SSP3-7.0 in 2050 to 8.0 years in SSP1-1.9 in 2050, which is lower than the 9.1-year lifetime calculated using observational data[58]. To avoid misrepresentations due to the low bias, we use the relative change in lifetime due to the transport

emissions instead of the absolute values and apply it to a range of CH_4 lifetime values reported in the literature (see 'Calculation of the methane and CO_2 effects'). This provides more reliable estimates of the absolute lifetime, with respect to transport-induced loss, and its uncertainties. When applying the classical perturbation method, commonly used in previous studies, instead of the tagging approach adopted here, the relative lifetime change resulting from transport emissions modelled here turns out to be very similar to previous studies[15], indicating the robustness of the EMAC results compared to other models.

Tagging concentrations of molecules with their sources enables the calculation of the transport effects based on a single simulation, instead of the two model runs required by the perturbation method used for the aerosol analysis. Note that we cannot apply the tagging approach for the aerosol effects yet due to the particular challenge of tagging aerosol-cloud interactions and liquid-phase chemistry. However, the consistency of the gas-phase and the aerosol simulations is very high. This is achieved by i) applying the same base model, ii) using the same data sets for anthropogenic and natural emissions (see below), retaining only slight differences in volcanic and lightning emissions, which could not be fully harmonized for technical reasons, and iii) using the same meteorological data to drive the model dynamics. In analogy to the aerosol simulations, the model dynamics of the gas-phase simulations were driven by meteorological reanalysis data applying the nudging technique. Since the interannual variability of the gas-phase chemistry in our simulations is considerably smaller than that of the aerosol effects, a shorter simulation period is sufficient. Here, simulations have been performed as time slice experiments for the period from July 2012 to December 2017, where the months in 2012 are used as model spin-up and only the years from 2013 to 2017 are analyzed. For the same reasons as for the aerosol simulations, the present-day meteorology is also applied in the simulations of the future scenarios. For more details on the model configuration, we refer to the accompanying article on the gas-phase effects[15]. Many previous studies of transport-induced effects on gas-phase chemistry relied on the perturbation method, as applied here for aerosol effects. However, due to particularly strong nonlinearities of the gas-phase chemistry, this method can suffer from large uncertainties in quantifications of transport-induced contributions to anthropogenic climate change. This triggered the development of the tagging approach[21,55] applied in the present study. Hence, the obtained results partly deviate from those of previous studies. For an analysis of these deviations, we refer to our previous articles on the gas-phase chemistry effects[15,21].

Calculation of the methane and CO_2 effects

While the concentrations of short-lived compounds show large spatial variation, long-lived greenhouse gases are relatively well mixed throughout the global atmosphere, resulting in a rather homogeneous spatial distribution. This implies that the transport sectors' effects on CH_4 and CO_2 can be well approximated on the basis of global mean concentrations. Hence, the great computational effort of full three-dimensional models can be avoided, and long-term simulations necessary to describe the accumulation of these compounds in the atmosphere can be carried out more efficiently. To calculate the transport-induced CH_4 and CO_2 effects, we applied the climate response model AirClim[50,59,60].

To adapt the model to the specific requirements of this study, we were able to take into account the results from the tagging approach as described in the following. The effect of transport emissions on atmospheric methane is calculated from the chemical loss due to reaction with the OH radical as simulated with EMAC in QCTM/TAGGING configuration (see above). The average loss rate is then converted to the transport-induced relative change in methane lifetime:

$$\delta = -\overline{loss\left(CH_4\right)^{tra}} / \overline{loss\left(CH_4\right)^{total}} \tag{1}$$

where $\overline{loss\left(CH_4\right)^{total}}$ represents the global multi-year mean total loss rate of CH_4 due to reaction with OH and $\overline{loss\left(CH_4\right)^{tra}}$ denotes the fractional loss rate due to reaction with OH resulting from transport emissions[56]. The lifetime change is calculated for the troposphere (here below the monthly-mean tropopause height), as the reaction with OH in the troposphere is the dominant CH_4 sink[61]. For more details on these calculations, we refer to the accompanying article on the gas-phase effects[15]. Following the tagging approach[55], the transport-related contribution to atmospheric methane is calculated via Euler backward time integration of the following equation from 1750 to the analyzed year:

$$\frac{\partial}{\partial t} CH_4^{tra} = -\frac{1}{2}\left(\frac{1}{\tau^{tra}} CH_4 + \frac{1}{\tau} CH_4^{tra}\right) \tag{2}$$

Here, CH_4 and CH_4^{tra} denote the total methane mixing ratio and the corresponding contribution of the respective transport sector, which is negative in case of a transport-induced loss. The symbols τ and τ^{tra} represent the methane lifetime corresponding to total chemical loss and to only transport-induced loss, with τ^{tra} calculated from $\delta = -\tau/\tau^{tra}$. Note that τ^{tra} does not represent the absolute change in τ due to the occurrence of transport emissions. It rather represents the chemical lifetime corresponding to the methane loss due to reaction with the fraction of OH resulting from transport. Hence, τ^{tra} can be much larger than τ. Since τ is subject to large uncertainties, we performed three simulations for each case (each transport sector along each of the three scenario pathways) assuming a methane lifetime of 7.5, 9, and 12 years to cover the range of values of τ reported in the literature[62]. Corresponding values for τ^{tra} are computed from δ. The full time series from 1750 to 2050 is derived from the 2015 and 2050 values, assuming a temporal evolution of δ that correlates with that of the respective NO_x emissions (see description of emission data below) and matches the values obtained from the EMAC simulations for 2015 and 2050. The resulting transport-related CH_4 contribution (negative) is then used to calculate the transport-induced radiative effects from the total CH_4 mixing ratios with and without the transport-induced contribution following Etminan et al.[63]. Information on the temporal evolution of the total CH_4 mixing ratio, the NO_x emissions and the N_2O mixing ratio, which is required for the radiation calculations, are taken from the CMIP6 data sets[64]. The transport-induced loss of methane also results in a reduced production of ozone, leading to an additional radiative forcing. According to previous studies, this is considered via enhancement of the methane radiative forcing by the factor 1.29 in AirClim[60].

The contribution of the respective transport sector emissions to the global mean CO_2 concentration CO_2^{tra} is calculated in AirClim from the globally aggregated, fossil fuel-related transport CO_2 emissions via a response function considering five different prescribed response times, which characterize different loss processes in the CO_2 life cycle. In a previous study[65], the CO_2 life cycle as simulated by AirClim was compared with the results of similar models, and a reasonable agreement was found. The spread of the results (deviations around 10-20%) is used here to define a corresponding uncertainty range (see 'Calculation of uncertainties'). To capture the long-term accumulation of CO_2 in the atmosphere, the temporal evolution of the transport emissions is considered, including both the historical emissions[1] and the future development of the emissions in the respective scenarios[2]. The time-dependent radiative forcing of the obtained transport-induced amount of CO_2 is then calculated as[66]:

$$RF_{CO_2}^{tra}(t) = f^{tra}(t) \cdot RF_{CO_2}^{ant}(t) \tag{3}$$

where $f^{tra}(t) = CO_2^{tra}(t)/(CO_2(t) - CO_2^0)$ is the fractional contribution of the respective transport-induced CO_2 to the total anthropogenic change in CO_2, calculated from the CO_2 concentrations[64] CO_2^0 and $CO_2(t)$ at a pre-industrial reference year (here 1750) and at later times, respectively. $RF_{CO_2}^{ant}(t)$ is the corresponding time-dependent total anthropogenic radiative forcing calculated from the total anthropogenic change in CO_2 as described by Ramaswamy et al.[42] (Table 6.2 in that publication, first row in descriptions of CO_2 effects).

Effects of contrail cirrus

The climate forcing of contrail cirrus clouds is the only transport impact that was not explicitly simulated in the present study, since essential input data, especially the flown distances per grid box, are not available in the CMIP6 emission data set. To provide a suitable estimate of the contrail cirrus effect in order to complement the set of effects analyzed here, we rely on results from previous studies[14,48,67]. A recent aviation climate assessment[14] reports a contrail cirrus ERF of 44.1 mW/m^2 in 2011 and 57.4 mW/m^2 in 2018. Assuming exponential growth between 2011 and 2018, this indicates a contrail cirrus ERF of 51.27 mW/m^2 in 2015. To estimate a corresponding 2050 value, we apply results from another study[48], where consistent quantifications of the contrail cirrus effect were provided for 2006 and 2050 based on a 2050 emission scenario derived from an expected growth of aviation transport volumes by a factor of 4 in that timeframe. From the obtained contrail cirrus radiative forcings of 49 mW/m^2 in 2006 and 160 mW/m^2 in 2050 (assumption of conventional fuels and technology), a value of 62.42 mW/m^2 in 2015 is determined, assuming exponential growth of transport volume and a linear relationship between transport volume and contrail cirrus radiative forcing. According to these radiative forcing values, we scale the 2015 ERF of 51.27 mW/m^2 derived from the recent assessment to 2050, resulting in an ERF of 131.42 mW/m^2. These values are used to calculate the total aviation ERF from the effects quantified here for 2015 and 2050 in the case of SSP3-7.0. For SSP2-4.5 and SSP1-1.9, the contrail cirrus ERF for 2050 is reduced by 20% and 50%, respectively, corresponding to the effects of a moderate and high degree of sustainability through the use of alternative fuels and technologies[67], in line with the storylines of these scenarios. However, it should be emphasized that this does not represent a concrete quantification of the contrail effects in the SSPs, but merely an estimate for scenarios of varying sustainability.

In a recent study[68], simulations were performed with the EMAC model in a very similar configuration to the one used here, including an explicit calculation of the radiative forcing from contrail cirrus based on an aviation emissions inventory containing all the parameters required for this purpose (Aviation Environmental Design Tool, AEDT[69]). The results show a radiative forcing (RF) of 60.7 mW/m^2 from contrail cirrus in 2006 and 188 mW/m^2 in 2050, assuming that air traffic quadruples in this time frame[48]. Assuming exponential growth, this results in an RF of 76.5 mW/m^2 for 2015. With a ratio of ERF to RF of 0.66, which was also quantified in that study[68], an ERF of 50.5 mW/m^2 can be estimated, which is very close to the ERF of 51.27 mW/m^2 derived here from the literature. The RF of 188 mW/m^2 simulated for 2050 implies an ERF of 124.1 mW/m^2, which is also quantitatively consistent with the literature-based ERF of 131.42 mW/m^2 assumed here for 2050 in the case of conventional fuels (SSP3-7.0, 2050). With regard to aviation fuel consumption, the AEDT inventory also appears to agree well with the CMIP6 inventory used here. This can be concluded from a comparison of the aggregated annual global CO_2 emissions in 2015, given that the CO_2 emission factor is well established. Based on the AEDT CO_2 emissions of 594.9 Tg in 2006, a value of 789.9 Tg can be estimated for 2015, assuming exponential growth and an increase in air traffic volume by a factor of 4 by 2050 compared to 2006. This agrees well with the 766.0 Tg of CO_2 emissions in the CMIP6 inventory for 2015. Therefore, we would expect very similar ERF values calculated with EMAC for CMIP6 if the missing parameters were available in this database. This indicates that a possible bias due to the use of literature-based values for the ERF of contrail cirrus in the present study is likely to be small. Hence, the literature-based ERF can be regarded as consistent and comparable with the ERF explicitly simulated for the other processes.

Emission data

Global distributions of anthropogenic and open burning emissions for 2015 and 2050 in the different scenarios were taken from the CMIP6 data set[1,2,34]. The CMIP6 data includes information on historical emissions between 1750 and 2014 and data on future developments covering the time period from 2015 to 2100. Here, we consider the year 2015 (from SSP2-4.5) for present-day simulations instead of the last year of the historical CMIP6 data set (2014) to use consistent information from the same emission database for present-day conditions and 2050. However, we stress that the differences between the 2014 and 2015 data, as well as between the 2015 data for the different future projections are negligible. Time series of globally aggregated annual emissions of CO_2 and NO_x from the transport sectors for the time period from 1750 to 2050, required for describing the transport-induced CO_2 and CH_4 effects, are taken directly from the CMIP6 data set for historical conditions[1] (until 2014) complemented by values aggregated from the gridded (spatially resolving) data[34] for the period 2015-2050. For the representation of emissions from other sources as described above, especially wind-driven natural particle emissions, volcanic emissions, and emissions from lightning and biogenic sources, we refer to the accompanying papers[15,16].

The applied emission data does not account for the effects of the COVID-19 pandemic, since the SSPs and the corresponding data were generated earlier. However, the pandemic has had a large impact, particularly on the transport sectors, and could also influence their future development. In the case of CO_2, the emissions quickly returned to levels similar to those before the pandemic and continued their upward trend[70]. The impact on the year 2050 is therefore expected to be low. It should also be noted that the future scenarios applied in the present study are mainly used to draw general conclusions about the transport effects at different levels of emissions, which implies that our results are not directly affected by neglecting the pandemic.

Harmonization of radiative forcing

Due to different processes to be considered, different methods for the calculation of the radiative forcings are applied. For the aerosol effects, the forcing is derived as the difference in top-of-atmosphere radiative fluxes from two model runs, one with and one without the aerosol effects of the respective transport sector emissions[16]. Since this difference also includes the effects of rapid adjustments, for instance, of clouds, it is regarded here as ERF[16,71]. In case of the ozone effect, the model calculations described above yield a stratospheric adjusted radiative forcing[42,43] (SARF) by means of the multiple radiation calling technique using the transport-induced ozone contributions determined via the tagging approach[15]. An ERF cannot be derived directly from these simulations, since the online calculations of model chemistry have to be decoupled from the model dynamics to enable the quantification of small perturbations (QCTM mode, see 'EMAC simulations' section). The method for calculating the methane effects outlined above also results in SARF values. To make these effects comparable to the aerosol effects and to enable summation of the effects to calculate the total forcings, the SARF values are converted into ERF, which has been widely accepted as the more advanced metric[42–44]. The conversion relies on a multi-model assessment of the ERF of anthropogenic changes in radiatively active species, including an analysis of the corresponding SARF[72]. We apply ratios of ERF and SARF of ozone changes due to anthropogenic emissions of ozone precursor gases, as well as ERF and SARF of anthropogenic changes in the methane concentration and the resulting chemical impact. For consistency, we only take into account the results of the assessment obtained from models with full interactive chemistry, with the exception of one model (MRI-ESM2) that is not considered as it shows an exceptionally low ERF-to-SARF ratio in case of the ozone effect. In case of ozone changes, we apply a mean ERF/SARF ratio of 0.97 and corresponding minimum and maximum ratios of 0.77 and 1.31, respectively, for the uncertainty range. For the methane effect, the corresponding ratios amount to 1.03, 0.88, and 1.23, respectively. For CO_2, we apply the approximation ERF/SARF $\sim$1, which is based on multi-model mean results from a recent analysis of different radiative forcing metrics based on the CMIP6 models[73].

Calculation of uncertainties

Chemistry-climate models and their input data are affected by different sources of uncertainties. Assessing the effects of all known uncertainties would require an integration of all results available from previous studies as provided, for instance, in a recent survey on the climate effects of aviation

emissions[14]. An extension of this assessment to land-based transport and shipping, however, is beyond the scope of the present study. Here, we focus only on those uncertainties directly resulting from the specific model approach applied.

Quantifications of aerosol effects on climate suffer from particularly high uncertainties[3,43]. This is also the case for transport-related aerosol effects, as demonstrated in one of our previous studies[20]. There, we showed that the effective radiative forcing of transport-induced aerosols can change by several 10% when the model assumptions on the size distributions of the emitted particles are varied. With this approach, we assessed the uncertainties arising from the transformation of aerosols near their sources, which cannot be adequately resolved by the large grid boxes of global models. To account for this in the present study, we adopt the corresponding uncertainties, which amount to ±75%, ±64%, and ±18% for land-based transport, aviation, and shipping, respectively. These values are based on the ERF calculated in the previous study for two different cases for each transport sector spanning a range of aging efficiencies of the respective transport-induced aerosol population. They are adopted to calculate uncertainties in terms of maximum and minimum values from the ERF modelled in the present study.

In the case of the transport-induced ozone contribution and the corresponding change in the OH concentration driving the methane effect, major uncertainties of our quantifications result from the conversion of SARF to ERF. Therefore, the minimum and maximum values of the ERF/SARF ratio described above are used as uncertainty ranges. In the case of the methane effect, the uncertainty in methane lifetime is also taken into account. In a first step, the SARFs of the transport-induced methane perturbations are calculated for the three different assumptions on methane lifetime (7.5, 9, and 12 years). In a second step, the resulting uncertainty range is further extended by including the minimum and maximum values of the conversion factors ERF/SARF by scaling the lowest and largest absolute SARF values with the minimum and maximum ERF/SARF ratios, respectively.

For the CO_2 effect, an uncertainty range of ±15% is assumed according to the uncertainty of the linear response model applied to simulate the carbon cycle in AirClim[59]. Uncertainties of the contrail effect, as derived, for instance, in the recent aviation assessment[14] from multiple model and parameter studies, are not included here, since this would result in an inconsistency with the uncertainties quantified in the present study which are based on simulations with a single model.

To determine the uncertainties of the overall effect of individual transport sectors or of transport as a whole, the uncertainties of the individual effects are combined. When summing the ERFs of the same process, the uncertainties are assumed to be correlated. In this case, they are determined as minimum or maximum values by summing the minimum or maximum values of the individual contributions. If the ERFs of different processes are added, it is assumed that the uncertainties are uncorrelated. In this case, they are combined by means of Gaussian error propagation.

Data availability

For the availability of output from the simulations of the aerosol-related effects performed with EMAC, including the aerosol submodel MADE3 and the corresponding output of the gas-phase chemistry simulations with EMAC in the QCTM/TAGGING mode, we refer to the two accompanying articles[15,16]. The ERF values and associated uncertainties resulting from the EMAC and AirClim simulations and their postprocessing are provided in the Supplementary information. The CMIP6 emission data applied in the simulations of this study (aggregated historical emission time series, gridded CMIP6 emission data) is available as described in the cited articles[1,34].

Code availability

The Modular Earth Submodel System (MESSy) is continuously developed and applied by a consortium of institutions. MESSy and the source code are licensed to all affiliates of institutions that are members of the MESSy Consortium. Institutions can become members of the MESSy Consortium by signing the MESSy Memorandum of Understanding. More information can be found on the MESSy Consortium website (http://www.messy-interface.org, last accessed: 31 January 2026). The model configurations applied in this study are based on EMAC version 2.55. The exact set-ups used to produce the results of this paper are archived at the German Climate Computing Center (DKRZ) and can be made available to members of the MESSy community upon request. The software code of AirClim is confidential proprietary information of DLR. Therefore, the code cannot be made available to the public or the readers without any restrictions. Licensing of the code to third parties is conditioned upon the prior conclusion of a licensing agreement with DLR as licensor. The codes used for analyzing the data and plotting the analyzed data are available from the corresponding author upon request.

Received: 5 December 2025; Accepted: 6 March 2026;
Published online: 11 April 2026

References

1. Hoesly, R. M. et al. Historical (1750–2014) anthropogenic emissions of reactive gases and aerosols from the Community Emissions Data System (CEDS). *Geosci. Model Dev.* **11**, 369–408 (2018).
2. Gidden, M. J. et al. Global emissions pathways under different socioeconomic scenarios for use in CMIP6: a dataset of harmonized emissions trajectories through the end of the century. *Geosci. Model Dev.* **12**, 1443–1475 (2019).
3. IPCC, Summary for Policymakers, in: *Climate Change 2021: The Physical Science Basis. Contribution of Working Group I to the Sixth Assessment Report of the Intergovernmental Panel on Climate Change* (eds. Masson-Delmotte, V. et al.) (Cambridge University Press, Cambridge, United Kingdom and New York, NY, USA, pp. 3−32, https://doi.org/10.1017/9781009157896.001, 2021).
4. ITF (International Transport Forum), *ITF Transport Outlook 2023*. https://doi.org/10.1787/b6cc9ad5-en (OECD Publishing, Paris, 2023).
5. IPCC, Summary for Policymakers, in: *Global Warming of 1.5 °C. An IPCC Special Report on the impacts of global warming of 1.5 °C above pre-industrial levels and related global greenhouse gas emission pathways, in the context of strengthening the global response to the threat of climate change, sustainable development, and efforts to eradicate poverty* (eds. Masson-Delmotte, V. et al.) (Cambridge University Press, Cambridge, UK and New York, NY, USA, pp. 3-24, https://doi.org/10.1017/9781009157940.001, 2018).
6. European Commission, *Communication from the Commission to the European Parliament, the Council, the European Economic and Social Committee and the Committee of the Regions*, A European Strategy for Low-Emission Mobility, COM (2016) 501 (2016).
7. EPA (United States Environmental Protection Agency), Revised 2023 and Later Model Year Light-Duty Vehicle Greenhouse Gas Emissions Standards. *Fed Regist* **86**, 74434–74526 (2021).
8. EPA (United States Environmental Protection Agency), Control of Air Pollution From New Motor Vehicles: Heavy-Duty Engine and Vehicle Standards. *Fed Regist* **87**, 17414–17888 (2022).
9. Manisalidis, I., Stavropoulou, E., Stavropoulos, A. & Bezirtzoglou, E. Environmental and Health Impacts of Air Pollution: A Review. *Front. Public Health* **8**, 14 (2020).
10. Molina, L. T. Introductory lecture: air quality in megacities. *Faraday Discuss* **226**, 9–52 (2021).
11. Niklaß, M. et al. *Integration of Non-CO2 Effects of Aviation in the EU ETS and under CORSIA, Final report, CLIMATE CHANGE 20/2020*, Environmental Research of the Federal Ministry for the Environment, Nature Conservation and Nuclear Safety. Report No. (UBA-FB) FB000270/ENG, 207pp., ISSN 1862-4804, https://www.umweltbundesamt.de/sites/default/files/medien/1410/publikationen/2020-07-28_climatechange_20-2020_integrationofnonco2effects_finalreport_.pdf (German Environment Agency, Dessau-Roßlau, Germany, 2019).

12. Grewe, V. et al. Mitigating the Climate Impact from Aviation: Achievements and Results of the DLR WeCare Project. *Aerospace* **4**, 34 (2017).
13. Grewe, V. et al. Evaluating the climate impact of aviation emission scenarios towards the Paris agreement including COVID-19 effects. *Nat. Commun.* **12**, 3841 (2021).
14. Lee, D. et al. The contribution of global aviation to anthropogenic climate forcing for 2000 to 2018. *Atmos. Environ.* **244**, 117834 (2021).
15. Mertens, M. et al. The contribution of transport emissions to ozone mixing ratios and methane lifetime in 2015 and 2050 in the Shared Socioeconomic Pathways (SSPs). *Atmos. Chem. Phys.* **24**, 12079–12106 (2024).
16. Righi, M., Hendricks, J. & Brinkop, S. The global impact of the transport sectors on the atmospheric aerosol and the resulting climate effects under the Shared Socioeconomic Pathways (SSPs). *Earth Syst. Dynam.* **14**, 835–859 (2023).
17. Uherek, E. et al. Transport impacts on atmosphere and climate: Land transport. *Atmos. Environ.* **44**, 4772–4816 (2010).
18. Hoor, P. et al. The impact of traffic emissions on atmospheric ozone and OH: results from QUANTIFY. *Atmos. Chem. Phys.* **9**, 3113–3136 (2009).
19. Balkanski, Y. et al. Direct radiative effect of aerosols emitted by transport: from road, shipping and aviation. *Atmos. Chem. Phys.* **10**, 4477–4489 (2010).
20. Righi, M., Hendricks, J. & Sausen, R. The global impact of the transport sectors on atmospheric aerosol: simulations for year 2000 emissions. *Atmos. Chem. Phys.* **13**, 9939–9970 (2013).
21. Mertens, M., Grewe, V., Rieger, V. S. & Jöckel, P. Revisiting the contribution of land transport and shipping emissions to tropospheric ozone. *Atmos. Chem. Phys.* **18**, 5567–5588 (2018).
22. Lauer, A., Eyring, V., Hendricks, J., Jöckel, P. & Lohmann, U. Global model simulations of the impact of ocean-going ships on aerosols, clouds, and the radiation budget. *Atmos. Chem. Phys.* **7**, 5061–5079 (2007).
23. Eyring, V. et al. Transport impacts on atmosphere and climate: shipping. *Atmos. Environ.* **44**, 4735–4771 (2010).
24. Partanen, A. I. et al. Climate and air quality trade-offs in altering ship fuel sulfur content. *Atmos. Chem. Phys.* **13**, 12059–12071 (2013).
25. Sofiev, M. et al. Cleaner fuels for ships provide public health benefits with climate tradeoffs. *Nat. Commun.* **9**, 406 (2018).
26. Yuan, T. et al. Abrupt reduction in shipping emission as an inadvertent geoengineering termination shock produces substantial radiative warming. *Commun. Earth Environ.* **5**, 281 (2024).
27. Kontovas, C. A. Integration of air quality and climate change policies in shipping: The case of sulphur emissions regulation. *Mar. Policy* **113**, 103815 (2020).
28. Collins, W. J. et al. AerChemMIP: quantifying the effects of chemistry and aerosols in CMIP6. *Geosci. Model Dev.* **10**, 585–607 (2017).
29. Lund, M. T. et al. A continued role of short-lived climate forcers under the Shared Socioeconomic Pathways. *Earth Syst. Dynam.* **11**, 977–993 (2020).
30. Szopa, S. et al. Short-Lived Climate Forcers, in: *Climate Change 2021: The Physical Science Basis. Contribution of Working Group I to the Sixth Assessment Report of the Intergovernmental Panel on Climate Change* (eds. Masson-Delmotte, V. et al.) (Cambridge University Press, Cambridge, United Kingdom and New York, NY, USA, pp. 817–922, https://doi.org/10.1017/9781009157896.008, 2021).
31. Fuglestvedt, J., Berntsen, T., Myhre, G., Rypdal, K. & Skeie, R. B. Climate forcing from the transport sectors. *Proc. Natl. Acad. Sci. USA* **105**, 454–458 (2008).
32. O'Neill, B. C. et al. The roads ahead: narratives for shared socioeconomic pathways describing world futures in the 21st century. *Glob. Environ. Change* **42**, 169–180 (2017).
33. Riahi, K. et al. The Shared Socioeconomic Pathways and their energy, land use, and greenhouse gas emissions implications: An overview. *Glob. Environ. Change* **42**, 153–168 (2017).
34. Feng, L. et al. The generation of gridded emissions data for CMIP6. *Geosci. Model Dev.* **13**, 461–482 (2020).
35. Fricko, O. et al. The marker quantification of the Shared Socioeconomic Pathway 2: A middle-of-the-road scenario for the 21st century. *Glob. Environ. Change* **42**, 251–267 (2017).
36. van Vuuren, D. P. et al. Energy, land-use and greenhouse gas emissions trajectories under a green growth paradigm. *Glob. Environ. Change* **42**, 237–250 (2017).
37. Rogelj, J. et al. Scenarios towards limiting global mean temperature increase below 1.5 °C. *Nat. Clim. Change* **8**, 325–332 (2018).
38. Rogelj, J. et al. Mitigation Pathways Compatible with 1.5 °C in the Context of Sustainable Development, in: *Global Warming of 1.5 °C. An IPCC Special Report on the impacts of global warming of 1.5 °C above pre-industrial levels and related global greenhouse gas emission pathways, in the context of strengthening the global response to the threat of climate change, sustainable development, and efforts to eradicate poverty* (eds. Masson-Delmotte, V. et al.) pp. 93–174. https://doi.org/10.1017/9781009157940.004 (Cambridge University Press, Cambridge, United Kingdom and New York, NY, USA, 2018).
39. Fujimori, S. et al. SSP3: AIM implementation of Shared Socioeconomic Pathway. *Glob. Environ. Change* **42**, 268–283 (2017).
40. O'Neill, B. C. et al. The Scenario Model Intercomparison Project (ScenarioMIP) for CMIP6. *Geosci. Model Dev.* **9**, 3461–3482 (2016).
41. Smith, T. W. P. et al. Third IMO Greenhouse Gas Study 2014, Tech. rep. https://www.imo.org/en/OurWork/Environment/Pages/Greenhouse-Gas-Studies-2014.aspx (International Maritime Organization, London, UK, 2014).
42. Ramaswamy, V. et al. Radiative forcing of climate change, in: *Climate Change 2001: The Scientific Basis. Contribution of Working Group I to the Third Assessment Report of the Intergovernmental Panel on Climate Change* (eds. Joos, F. & Srinivasan, J.) https://www.ipcc.ch/report/ar3/wg1/ (Cambridge University Press, Cambridge, United Kingdom and New York, NY, USA, 2001).
43. Myhre, G. et al. Anthropogenic and Natural Radiative Forcing, in: *Climate Change 2013: The Physical Science Basis. Contribution of Working Group I to the Fifth Assessment Report of the Intergovernmental Panel on Climate Change* (eds. Stocker, T. F. et al.) https://www.ipcc.ch/report/ar5/wg1/ (Cambridge University Press, Cambridge, United Kingdom and New York, NY, USA, 2013).
44. Forster, P. et al. The Earth's Energy Budget, Climate Feedbacks, and Climate Sensitivity, in: *Climate Change 2021: The Physical Science Basis. Contribution of Working Group I to the Sixth Assessment Report of the Intergovernmental Panel on Climate Change* (eds. Masson-Delmotte, V. et al.) (Cambridge University Press, Cambridge, United Kingdom and New York, NY, USA, pp. 923–1054, https://doi.org/10.1017/9781009157896.009, 2021).
45. Thompson, A. The Oxidizing Capacity of the Earth's Atmosphere: Probable Past and Future Changes. *Science* **256**, 1157–1165 (1992).
46. Kaiser, J. C. et al. Global aerosol modeling with MADE3 (v3.0) in EMAC (based on v2.53): model description and evaluation. *Geosci. Model Dev.* **12**, 541–579 (2019).
47. Righi, M., Hendricks, J. & Beer, C. G. Exploring the uncertainties in the aviation soot–cirrus effect. *Atmos. Chem. Phys.* **21**, 17267–17289 (2021).
48. Bock, L. & Burkhardt, U. Contrail cirrus radiative forcing for future air traffic. *Atmos. Chem. Phys.* **19**, 8163–8174 (2019).
49. Manshausen, P., Watson-Parris, D., Christensen, M. W., Jalkanen, J.-P. & Stier, P. Invisible ship tracks show large cloud sensitivity to aerosol. *Nature* **610**, 101–106 (2022).
50. Hendricks, J. et al. Quantifying the climate impact of emissions from land-based transport in Germany. *Transp. Res. Part D. Transp. Environ* **65**, 825–845 (2018).
51. Morton, O. Is this what it takes to save the world?. *Nature* **447**, 132–136 (2007).

52. Jöckel, P. et al. Earth System Chemistry integrated Modelling (ESCiMo) with the Modular Earth Submodel System (MESSy) version 2.51. *Geosci. Model Dev.* **9**, 1153–1200 (2016).
53. Righi, M. et al. Coupling aerosols to (cirrus) clouds in the global EMAC-MADE3 aerosol–climate model. *Geosci. Model Dev.* **13**, 1635–1661 (2020).
54. Koffi, B., Szopa, S., Cozic, A., Hauglustaine, D. & van Velthoven, P. Present and future impact of aircraft, road traffic and shipping emissions on global tropospheric ozone. *Atmos. Chem. Phys.* **10**, 11681–11705 (2010).
55. Grewe, V., Tsati, E., Mertens, M., Frömming, C. & Jöckel, P. Contribution of emissions to concentrations: the TAGGING 1.0 submodel based on the Modular Earth Submodel System (MESSy 2.52). *Geosci. Model Dev.* **10**, 2615–2633 (2017).
56. Rieger, V. S., Mertens, M. & Grewe, V. An advanced method of contributing emissions to short-lived chemical species (OH and HO_2): the TAGGING 1.1 submodel based on the Modular Earth Submodel System (MESSy 2.53). *Geosci. Model Dev.* **11**, 2049–2066 (2018).
57. Naik, V. et al. Preindustrial to present-day changes in tropospheric hydroxyl radical and methane lifetime from the Atmospheric Chemistry and Climate Model Intercomparison Project (ACCMIP). *Atmos. Chem. Phys.* **13**, 5277–5298 (2013).
58. Prather, M. J., Holmes, C. D. & Hsu, J. Reactive greenhouse gas scenarios: Systematic exploration of uncertainties and the role of atmospheric chemistry. *Geophys. Res. Lett.* **39**, L09803 (2012).
59. Grewe, V. & Stenke, A. AirClim: an efficient tool for climate evaluation of aircraft technology. *Atmos. Chem. Phys.* **8**, 4621–4639 (2008).
60. Dahlmann, K., Grewe, V., Frömming, C. & Burkhardt, U. Can we reliably assess climate mitigation options for air traffic scenarios despite large uncertainties in atmospheric processes?. *Transp. Res. Part D. Transp. Environ.* **46**, 40–55 (2016).
61. Saunois, M. et al. Global Methane Budget 2000–2020. *Earth Syst. Sci. Data* **17**, 1873–1958 (2025).
62. Li, Q. et al. Reactive halogens increase the global methane lifetime and radiative forcing in the 21st century. *Nat. Commun.* **13**, 2768 (2022).
63. Etminan, M., Myhre, G., Highwood, E. J. & Shine, K. P. Radiative forcing of carbon dioxide, methane, and nitrous oxide: A significant revision of the methane radiative forcing. *Geophys. Res. Lett.* **43**, 12614–12623 (2016).
64. Meinshausen, M. et al. The shared socio-economic pathway (SSP) greenhouse gas concentrations and their extensions to 2500. *Geosci. Model Dev.* **13**, 3571–3605 (2020).
65. Sausen, R. & Schumann, U. Estimates of the climate response to aircraft CO_2 and NO_x emissions scenarios. *Clim. Change* **44**, 27–58 (2000).
66. Boucher, O., Borella, A., Gasser, T. & Hauglustaine, D. On the contribution of global aviation to the CO_2 radiative forcing of climate. *Atmos. Environ.* **267**, 118762 (2021).
67. Burkhardt, U., Bock, L. & Bier, A. Mitigating the contrail cirrus climate impact by reducing aircraft soot number emissions. *npj Clim. Atmos. Sci.* **1**, 37 (2018).
68. Bickel, M. et al. Contrail Cirrus Climate Impact: From Radiative Forcing to Surface Temperature Change. *J. Clim.* **38**, 1895–1912 (2025).
69. Wilkerson, J. T. et al. Analysis of emission data from global commercial aviation: 2004 and 2006. *Atmos. Chem. Phys.* **10**, 6391–6408 (2010).
70. United Nations Environment Programme. Emissions Gap Report 2024: No more hot air … please! With a massive gap between rhetoric and reality, countries draft new climate commitments, Nairobi, https://doi.org/10.59117/20.500.11822/46404 (2024).
71. Forster, P. M. et al. Recommendations for diagnosing effective radiative forcing from climate models for CMIP6. *J. Geophys. Res. Atmos* **121**, 12460–12475 (2016).
72. Thornhill, G. D. et al. Effective radiative forcing from emissions of reactive gases and aerosols – a multi-model comparison. *Atmos. Chem. Phys.* **21**, 853–874 (2021).
73. Smith, C. J. Effective radiative forcing and adjustments in CMIP6 models. *Atmos. Chem. Phys.* **20**, 9591–9618 (2020).
74. Feichter, J. et al. Simulation of the tropospheric sulfur cycle in a global climate model. *Atmos. Environ.* **30**, 1693–1707 (1996).
75. Li, R. L., Studholme, J. H. P., Fedorov, A. V. & Storelvmo, T. Precipitation efficiency constraint on climate change. *Nat. Clim. Chang.* **12**, 642–648 (2022).
76. Anderson, M., Salo, K. & Fridell, E. Particle- and Gaseous Emissions from an LNG Powered Ship. *Environ. Sci. Technol.* **49**, 12568–12575 (2015).

Acknowledgements

We are grateful to Axel Lauer (DLR), Anja Schmidt (DLR), Angelika Schulz (DLR), and Silvia Hendricks for their valuable comments on the manuscript. We would like to thank Ulrike Burkhardt (DLR) for very helpful discussions on the consideration of contrail cirrus effects, Sigrun Matthes (DLR) for her valuable comments on the model results for the aviation sector, and Vanessa S. Rieger (formerly DLR) for her contributions to the code for the calculation of methane effects. The processing of the CMIP6/SSP emissions for usage in EMAC has greatly benefited from the efforts of Markus Kunze and Phoebe Graf (both formerly DLR). This study was supported by the DLR transport research program through the projects TraK (Transport and climate), DATAMOST (Data and model-based solutions for the transformation of mobility), and MoDa (Models and Data for Future Mobility_Supporting Services). The model simulations and data analysis for this work used the resources of the Deutsches Klimarechenzentrum (DKRZ) granted by its Scientific Steering Committee (WLA) under project ID bd0080 and datasets provided by the MESSy community via the DKRZ data pool.

Author contributions

J.H. conceived the study, designed the simulations, prepared input data for AirClim, integrated and analyzed the model data, and wrote the paper. M.R. conceived the study, prepared input data for AirClim, designed and performed the EMAC simulations of the aerosol effects, analyzed the output data, and contributed to the text. S.B. processed the CMIP6/SSP emission data used to drive the model simulations, analyzed the model data, and contributed to the text. K.D. and J.C.K. performed the AirClim simulations, analyzed the output data, and contributed to the text. M.M. conceived the study, designed and performed the EMAC gas-phase chemistry simulations, analyzed the output data, and contributed to the text. C.G.B. integrated and analyzed the model output data and contributed to the text. V.G. and M.P. conceived the study and contributed to the text. All authors have approved the final version of the manuscript.

Funding

Open Access funding enabled and organized by Projekt DEAL.

Competing interests

The authors declare no competing interests.

Additional information

Supplementary information The online version contains supplementary material available at https://doi.org/10.1038/s41612-026-01383-y.

Correspondence and requests for materials should be addressed to Johannes Hendricks.